Green Chemistry

PAPER

View Article Online
View Journal | View Issue

Cite this: *Green Chem.*, 2020, **22**, 455

A sustainable preparation of catalytically active and antibacterial cellulose metal nanocomposites *via* ball milling of cellulose†

Joanna Kwiczak-Yiğitbaşı, [a] Özge Laçin,[a] Mine Demir, [a] Recep Erdem Ahan, [b] Urartu Özgür Şafak Şeker [b] and Bilge Baytekin [*a,b]

Cellulose, the most abundant polymer on Earth, and its composites have recently gained importance for the production of sustainable materials. These materials should be produced using green methods that avoid the utilization of toxic chemicals to ensure integrity for environmental sustainability. Ball milling, which gives a straightforward and (often) green synthetic access to materials, can be used to achieve this goal. Previously, it was shown that mechanochemical bond breakages in polymers generate mechanoradicals, which can be used to drive further reactions and to form polymer composites. In this study, we show that cellulose mechanoradicals generated during the ball milling of cellulose can reduce various metal ions to the corresponding metal nanoparticles (NPs) (Au, Ag, Pt, Pd, Co, and Cu), which are deposited and stabilized in the cellulose matrix. Using mechanoradicals to reduce the metal ions and form the cellulose composites, (1) the number of synthetic steps is reduced, and (2) the conventionally used, toxic reducing and stabilizing agents are avoided, which also prevents the contamination of the composites. The cellulose–metal nanoparticle composites can exhibit a wide range of properties that depend on the metal nanoparticle in the composite; *e.g.*, Au–cellulose nanocomposites exhibit catalytic activity, and Ag–cellulose nanocomposites exhibit antibacterial properties. The ball-milling method also permits blend formation using synthetic polymers, which allows tuning the physical properties of the final material. Finally, the method shown here provides a quick access to versatile metal nanoparticle cellulose composites (and their blends), which may find applications, such as in paper-based diagnostics and catalysis.

Received 7th August 2019,
Accepted 26th November 2019

DOI: 10.1039/c9gc02781e

rsc.li/greenchem

Introduction

Cellulose is the most abundant biopolymer in nature. It consists of a linear chain of D-glucose units linked by β-1,4-glycosidic bonds.[1,2] In the past few decades, this polysaccharide received considerable attention mostly because it is obtained from renewable and sustainable resources, which provides environmental benefits. Choosing natural polymers such as cellulose for some applications rather than a synthetic polymer is of great importance due to the rising problems of petroleum deficiency and environmental pollutions coming from the non-degradable synthetic polymers. Cellulose possesses other desirable properties, such as strength, stiffness, high thermal stability, and low cost due to worldwide availability.[3] Cellulose serves as a non-abrasive and non-toxic matrix in its composites, and provides a low-density and low-weight final material.[4,5] Another way of obtaining materials with improved properties with cellulose is blending it with the commonly used synthetic polymers. For example, the incorporation of cellulose fibers into thermoplastics enhances the stiffness and strength of the plastics.[6] Cellulose fibers come from renewable resources; they produce no health hazards and include biodegradability in the materials.[7] For example, cellulose fibers used in the preparation of artificial glass made of poly(methyl methacrylate) (PMMA) minimize the harm caused by ultraviolet radiation.[8] On the other hand, introducing a polymer into the cellulose matrix can modify the surface properties such as hydrophobicity.[9]

Among a wide variety of cellulose-based composites,[10–16] cellulose–metal (nano)composites have recently gained attention. Noble metal nanoparticles are commonly used in medicine,[17,18] biology[18] or industry.[19] Depending on the metal type, their composites are used in antibacterial textiles and kitchenware,[20] medical devices,[21] and electronic parts.[22] Recently, the cellulose nanocomposites have also started to find applications in paper diagnostics and paper electronics.[23,24]

[a]*Chemistry Department, Bilkent University, 06800 Ankara, Turkey. E-mail: b-baytekin@fen.bilkent.edu.tr*
[b]*UNAM, Bilkent University, 06800 Ankara, Turkey*

†Electronic supplementary information (ESI) available. See DOI: 10.1039/c9gc02781e

The cellulose–metal NP composites exhibit certain properties, for example, cellulose–silver nanoparticle composites can be used as an antibacterial material.[25,26] Another common use of cellulose–metal NP composites is the catalysis of organic reactions.[27] Generally, gold nanoparticles (Au NPs)[28–30] are used as the catalytic component; however, composites bearing palladium (Pd NPs),[31] or silver nanoparticles (Ag NPs)[32] are also reported to act as catalysts. Since metal NPs tend to aggregate to reduce their surface energy, they are generally stabilized by low molecular weight stabilizers (*e.g.*, thiols), chemical attachment to polymer surfaces or by simple capping using polymer chains. The former two methods require extra preparation steps and usually cause contamination of the final composite, which is vital if the composite material is to be used in analytical applications, *i.e.*, in biological or chemical sensing or diagnostics. In the latter case, NPs stabilized by the functional groups of the polymer may result in their poor accessibility towards the substrates.[33] Of the many matrix choices for nanocomposites, cellulose is a perfect matrix candidate, since it provides the necessary stabilization of NPs and provides a straightforward diffusion of the reagents to NPs.

In order to prepare cellulose–metal nanocomposites, many methods were developed.[34–38] However, one of the most widely used procedures is based on the reduction of metal ions in the cellulose matrix by a reducing agent in the presence of stabilizers.[39–41] This conventional preparation method involves toxic and hazardous solvents and reagents. Moreover, this non-environmentally friendly process is usually time-consuming and leads to contamination, which is detrimental in later applications, as mentioned above. A mechanochemical approach, which uses green chemistry principles,[42–44] stands as a better alternative to prepare cellulose–metal nanoparticle composites. It has already been successfully utilized in the direct synthesis of nanoparticles,[45–48] functionalization of cellulose,[49–51] and preparation of composite catalysts.[52,53]

In this study, we show the preparation of cellulose–metal nanocomposites (cellulose–Au, Ag, Pd, Pt, Cu, and Co) by activation of cellulose (cotton and microcrystalline cellulose (MCC)) by cryomilling (Scheme 1). This method uses no reducing and stabilizing agents – only cellulose, metal ion precursors and a few milliliters of water or acetonitrile (the latter is used only when the metal precursor is not well-soluble in water, and thus can be avoided by using different counter ions *etc*. in the metal precursors) are used. The method starts with the generation of peroxy mechanoradicals by covalent bond breakages upon milling.[54] The generation of mechanoradicals was reported many times in the literature for synthetic polymers and cellulose by us[51,55] and others.[49,56] These mechanoradicals play an essential role in the stabilization of other chemical species on polymer surfaces.[57]

We have also shown that lab scale chemical reactions can be driven by mechanoradicals, from nanoparticle synthesis to dye bleaching.[55,58,59] Here we also use the same strategy to create cellulose mechanoradicals,[49,56] and use them in the reduction of metal ions to obtain cellulose metal nanocomposites. The selection of the metal ions used was made to ensure an efficient reduction by the cellulose mechanoradicals (low standard reduction potential) and to provide a group of composites with different properties, *i.e.*, catalytic and antibacterial properties.

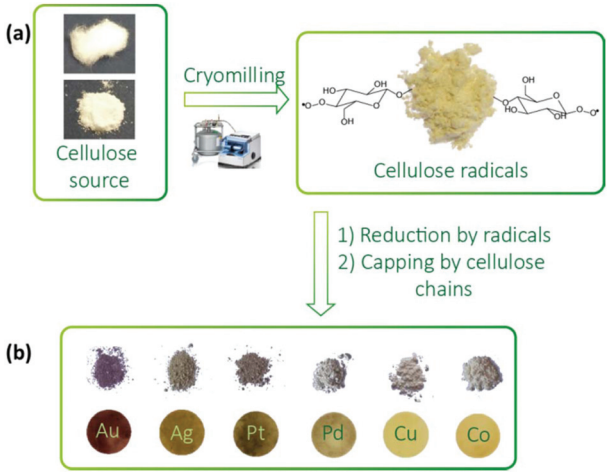

Scheme 1 Preparation of cellulose–metal nanocomposites. (a) MCC or cotton was cryomilled for 30 minutes at 30 Hz frequency at 77 K. (b) Solutions of $AgNO_3$, $HAuCl_4$, K_2PtCl_4 (3 mL, 5.1 mM, in H_2O), $Pd(C_5H_7O_2)_2$, $Co(C_5H_7O_2)_2$, and $Cu(C_5H_7O_2)_2$ (3 mL, 5.1 mM, in acetonitrile) were added on cryomilled cellulose (MCC or cotton) to form the metal nanoparticles in the cellulose matrix. The pellets were pressed from the corresponding powder after milling, which provides a practical storage and use of the final composite materials.

Using niche examples, we show that the prepared cellulose metal (Au, Ag, Pd, and Pt) nanocomposites can act as functional materials, according to the chemistry of the metal they contain: with Au, Ag, Pt, and Pd NPs, we catalyze the 4-nitrophenol reduction, and with Ag NPs, we present the antibacterial action towards *E. coli* (Gram-negative bacteria) and *B. subtilis* (Gram-positive bacteria). Besides, we report the preparation of cellulose–poly(methyl methacrylate) and cellulose–polystyrene blends by cryomilling, and the formation of Au nanoparticles in these blends, which eventually yields cellulose polymer–metal nanocomposites. Blending offers the tuning of physical properties; *e.g.* for these 'ternary' nanocomposites, we show the adjustment of the contact angle by altering the blend composition, as we show in one example with polystyrene.

Results and discussion

Synthesis and characterization of cellulose–metal nanocomposites

In all our nanocomposite preparations, we used two kinds of cellulose samples, microcrystalline cellulose (MCC) (Sigma-Aldrich) and conventional cotton. In order to mechanochemically activate the cellulose samples and to obtain the mechanoradicals, we use a cryomill (Retsch, Fig. S1†), which is ideal for milling the samples under cryo conditions and suppresses the thermally activated reactions during the mechanical input

and prevents the sticking of the polymer and cellulose samples. In a typical preparation, the samples were milled for 30 min at 30 Hz. This milling time was previously optimized to yield the highest amount of radicals per gram of cellulose (2.65×10^{18} and 3.25×10^{18} for cellulose and MCC, respectively, determined using the diphenylpicrylhydrazyl, DPPH assay).[60] The accompanying structural changes in the cellulose were elaborated in our previous study,[60] *i.e.*, we showed the accompanying decrease in the molecular weight of cellulose (for cotton and MCC, 2.4 and 1.4 times the original molecular weight, respectively) upon grinding for 30 min.[60] The chemical and morphological changes and the reduction in the particle size of the cellulose monitored by SEM, XRD, and ATR were also reported previously.[60] After cryomilling of cotton or MCC, metal ion solution (3 mL, 5.1 mM) was added onto a ground-cellulose sample and the mixtures were stored in the dark. For analysis, small parts of the samples were drawn after one day, one week, and two weeks, and they were washed to get rid of the metal precursor solution and dried. During the waiting time, the cellulose powder changed its colour from white to purple (Au NPs), to brown (Ag NPs), to grey (Pt NPs and Pd NPs), and to yellow (Cu NPs and Co NPs), reflecting the formation of metal nanoparticles in the cellulose matrix.

The SEM images of cellulose samples showed the NP formation (bright spots in the darker cellulose matrix); *e.g.* cotton-Au NPs (Fig. 1a and S2†) formed after one day. In the case of other metals, to obtain a similar deposition concentration of nanoparticles, longer storage times were necessary (as also proven by the XPS measurements, Table S1†). As seen in the SEM images, the nanoparticles (*ca.* 30–60 nm in size) were distributed in cellulose matrices (Fig. 1a and S3–S7†) and did not grow larger with longer waiting times. Even after waiting for months, the nanoparticles did not aggregate into larger particles, which indicated that the nanoparticles were well stabilized in fibrous and porous cellulose matrices due to secondary bonding (weak interactions) between the NPs and the hydroxyl and ether groups of the cellulose structure.[61] Similar images were obtained for MCC milled and stored with metal precursors under identical conditions (Fig. S8†). EDX spectra (Fig. 1a and S9†) showed the presence of an Au atom (signal at 2.12 eV), Ag atom (signal at 2.984 eV), Pt atom (2.048 eV), Pd atom (2.828 eV), and no signals arising from the corresponding counter ions in the metal ion precursors, which confirmed that the deposited material is free from the precursor. In order to confirm that the deposited material is in the reduced metallic form, we performed high-resolution X-ray photoelectron spectroscopy (HIRES XPS). The spectra displayed only signals from the metallic forms of Au(0), Ag(0), Pt(0) and Pd(0) NPs for both MCC and cotton nanocomposites (Fig. 1b, S10 and S11†). In the control experiments with the samples, which are not milled but allowed to stay in the metal ion solutions, there was no deposition of the metal (reduced metal or the metal precursors), as verified by HIRES XPS.

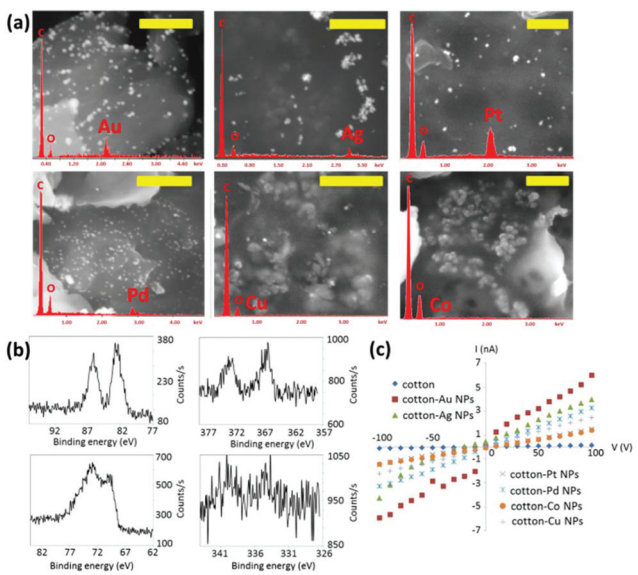

Fig. 1 (a) The EDX spectra (shown in red) of cotton-metal nanocomposites after 1 week of their storage in different metal salt solutions. All types of nanocomposites were imaged by SEM (Au, top left; Ag, top middle; Pt, top right; Pd, bottom left; Cu, bottom middle; and Co, bottom right). Scale bar = 500 nm. (b) XPS spectra of cotton-Au (top left); -Ag (top right); -Pt (bottom left); and -Pd (bottom right). (c) Current–voltage plot presenting increased electrical surface conductivity of nanocomposites in comparison with cotton (for details, see the Experimental section).

In parallel, X-ray diffraction (XRD) analysis (Fig. S12 and S13†) of these samples showed the diffraction peaks arising from the metallic lattices. In the case of cellulose–Cu and cellulose–Co nanocomposites, although the SEM showed the formation of some nanoparticles, the concentration of nanoparticles was low even after 2 weeks of waiting time in the metal precursor solution, which led to the difficulties in their analysis by EDX (Fig. 1a and S9†), XPS (Fig. S14†) or XRD (Fig. S15†). Therefore, it was challenging to identify the exact oxidation state of Co and Cu NPs. However, due to the lack of XPS signals of the counter ion of the metal precursor, and taking the previous results on synthetic polymer/Cu nanocomposites into account,[58] we surmise that the metal NPs are likely to form when cellulose mechanoradicals reduce Cu^{2+} and Co^{2+} ions to their metallic forms. Then, some of the Cu^0 and Co^0 might be oxidized by atmospheric oxygen to form stabilized CuO and CoO NPs. The chemical mechanism of metal ion reduction includes the oxidation of cellulose[62] and may be proposed as shown in Fig. S16.† This mechanism is additionally supported by the FTIR-ATR spectra showing that during grinding and after the addition of the metal ion precursors a new signal at 1650 cm^{-1} (C=O stretching) appeared (Fig. S17 and S18†). (This increase in the carbonyl groups also helps in effective capping of the metal nanoparticles in the cellulose matrix.)

The atomic percentages of metals in the nanocomposites were estimated by XPS measurements (for details, see the ESI text and Table S1†). The atomic percentages of metals in cotton composites indicated that the deposition of Au is fast and does not significantly increase during the waiting time in

the metal ion solution (0.148%, 0.176%, and 0.184%, after one day, one week, and two weeks, respectively). However, for cotton-Ag, and -Pt nanocomposites, increasing the waiting time of cryomilled cotton in the metal ion solution increased the metal content of the composites: from 0.013% to 0.167% (Ag), and from 0.051% to 0.142% (Pt) after two weeks, slowing down after 1 week, by which the number of mechanoradicals reaching the surface and reacting level out with respect to the waiting time, Fig. S19.†[60] The yields of metal ion to metal NP conversion were calculated based on the ICP-MS measurements (Table S2†) and the initial concentration of the metal ion solution used. These were found to be 62.4%, 53.9%, 12.1%, and 3.7%, for MCC-Au, -Pt, -Ag, and -Pd, respectively. For cotton-Au, -Pt, -Ag, and -Pd, the corresponding conversion yields were determined as 81.6%, 52.6%, 8.5%, and 3.7%.

We also pressed 70 mg of each powdered composite into pellets with 1 cm diameter using a sample pellet press. Pelleting the composite powders did not change the chemical nature and crystallinity of the composites as shown in their XPS spectra and XRD diffractograms (Fig. S20 and S21†). The electrical conductivity measurements of these pellets show up to 40-fold increase in conductivity upon the formation of nanoparticles in the cellulose samples, Fig. 1c (for details, see the Experimental section and Table S3†). Nevertheless, for practical applications of these nanocomposites, *e.g.*, as conductive papers, higher conductivities are required, for which the preparation procedures should be optimized to obtain a higher doping of the metals.[23]

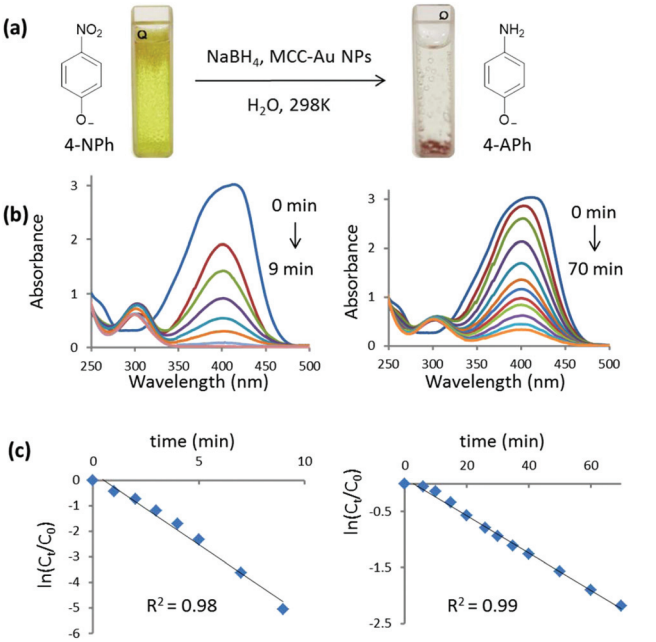

Fig. 2 (a) Reduction of 4-NPh (3 mL, 0.3 mM in H_2O) to 4-APh with MCC-Au NPs (1.0 mg composite in powder form). (b) UV-Vis absorption spectra during the first (left) and second (right) catalytic cycles in the presence of MCC-Au NPs. (c) The reaction is first order as shown by the linear $\ln(C_t/C_0)$ *vs.* time plots in the 1st (left) and 2nd (right) cycles of the reaction, performed under identical conditions. (For details on the reaction conditions, see the Experimental section.)

The catalytic activity of cellulose metal nanocomposites

In order to test the catalytic activity of the nanocomposites, we chose the reduction reaction of 4-nitrophenolate (4-NPh) to 4-aminophenolate (4-APh) using $NaBH_4$. Owing to the straightforward monitoring of the reaction by UV-Vis spectroscopy, this reaction is widely used to probe the catalytic activity in cellulose metal composites, in which the metal NPs are stabilized using chemicals.[28] We used powders of MCC metal nanocomposites (MCC-Au, MCC-Pd, MCC-Pt or MCC-Ag) as catalysts.

In a typical experiment, $NaBH_4$ (0.375 mL, 0.47 M in H_2O) was introduced into a solution of 4-NPh (3 mL, 0.30 mM in H_2O); the mixture became bright yellow and an absorbance band with a maximum at 400 nm in the UV-Vis spectrum was observed due to the formation of 4-nitrophenolate anion (Fig. 2a and b). After the addition of MCC metal nanocomposite powder (metal content in 1.0 mg of composite: 3.76 μg (Au), 0.20 μg (Ag), 0.12 μg (Pd), and 3.22 μg (Pt), Table S2†) to the mixture, the absorbance at 400 nm decreased, while a new peak appeared at 300 nm showing the formation of 4-aminophenolate (Fig. 2b and S22†). Without the addition of the catalyst, no significant reduction of 4-NPh was observed. The catalysed reaction followed first-order kinetics as evidenced from the linear plot $\ln(C_t/C_0)$ *vs.* time (Fig. 2c and S22†).[63]

XPS spectra of the samples before (Fig. S11†) and after catalysis (Fig. S23†) confirm that the nanoparticles remain in their metallic form and do not oxidize during the catalysis. In order to show that the MCC metal nanocomposites are reusable in the consecutive catalytic process, MCC-Au NP powders recovered by filtration after the reduction of 4-NPh were washed and dried, and were subjected to a consecutive reaction cycle (Fig. 2b and c). The rate constant for the transformation of 4-nitrophenolate into 4-aminophenolate in this second cycle was found to be 0.034 ± 0.002 min^{-1}. (The first cycle's rate constant was 0.501 min^{-1}.) This can be explained by the ICP-MS measurements, which indicated that the content of gold in 1.0 mg of composite decreased from 3.76 μg to 3.60 μg (after the 1st catalytic cycle) and 3.46 μg (after the 2nd catalytic cycle) (Table S2†). This decrease might be because of the conformational changes of the cellulose chains upon the absorption of water, which allows some of the adsorbed (chain-trapped) NPs to leak out into the solution. Such a leakage can be prevented by using pellets (Scheme 1) or a chemical binder of cellulose to retain the solid state conformation of the chains also in the wet state.

We tried to make a comparison between our composite material's catalytic performance with the literature values reported for similar cellulose metal nanocomposites, which had been formed by the conventional method and that are used for catalysing the same reaction (Table 1). The reaction rate of the 4-nitrophenolate reduction catalysed by polymer metal nanoparticles depends on many factors such as the nanoparticle size and shape and the type of polymeric support

Table 1 Comparison of the cellulose-based nanocatalysts in the reduction of 4-NP

Entry	Catalyst	Temp. [K]	Molar ratio			k [min^{-1}]	Ref.
			$NaBH_4$	4-NP	Metal		
1	Au/PDDA/NCC[a]	298	36 585	37	1	0.306	28
2	AuNPs@CSNFs[b]	298	22 000	22	1	0.354	29
3	AuNPs@CNs[c]	298	9720	30	1	0.124	30
4	MCC-Au NPs	298	2200	11	1	0.501 ± 0.060	This work
5	CNC@PDA-Ag[d]	298	30 810	97	1	0.255	32
6	MCC-Ag NPs	298	1980	10	1	0.174 ± 0.080	This work
7	PdNPs@CNs[e]	298	475 000	150	1	0.342	31
8	MCC-Pd NPs	298	6655	34	1	0.172 ± 0.015	This work
9	MCC-Pt NPs	298	990	5	1	0.127 ± 0.020	This work

[a] Au NPs on poly(diallyldimethylammonium chloride)-coated nanocrystalline cellulose. [b] Au NPs on crystalline cellulose nanofibers. [c] Au NPs on cellulose nanocrystals. [d] Ag NPs on polydopamine-coated cellulose nanocrystals. [e] Pd NPs on cellulose nanocrystals.

or stabilizing agents,[27,28] and therefore, our comparison is only rough. Our MCC-Au nanocomposite exhibited much higher catalytic activity than the cellulose nanocrystal or nanofiber nanocomposites (Table 1, entries 1–4) (reaction was also conducted in the flask under constant stirring. The expected transformation occurred within 8.5 min and the rate constant was equal to 0.531 ± 0.028 min^{-1} (see the Experimental section and Fig. S24†)). However, for both MCC-Ag (Table 1, entry 6) and MCC-Pd (Table 1, entry 8) nanocomposites, lower catalytic performance was obtained in comparison with the NPs coated on cellulose nanocrystals (Table 1, entries 5 and 7). To the best of our knowledge, there is only one report on catalytic action of cellulose Pt nanocomposites used in the reduction of 4-NPh. However, there is no reported data for the value of the rate constant, therefore, a comparison with our composites was not possible.[64] Avoiding the conventional routes which usually require a stabilizer or other chemicals for the production of metal NPs allowed a good access to the surface of the metal nanoparticles, as evident from the comparison of the catalytic activities of the conventionally and mechanochemically formed nanocomposites. These results clearly suggest that the latter can be used in the catalytic processes as a sustainable material.

Antimicrobial activity of cellulose–Ag nanocomposites

Another promising application for cellulose metal nanoparticle composites is their use as antibacterial materials, *e.g.* in food packaging or textiles.[21] A simple display of such an activity with our mechanochemically obtained cellulose metal nanocomposites bearing Ag metal NPs is as follows: silver nanoparticles are considered as broad spectrum antimicrobial agents with minimal toxicity to humans.[65] The antimicrobial activity of such mechanochemically prepared cellulose–Ag nanocomposites was determined using an agar disk assay against *E. coli* (Gram-negative bacteria) and *B. subtilis* (Gram-positive bacteria); two of the most characterized organisms among the Gram-positive and Gram-negative species. The experiments with cotton and MCC Ag nanocomposites were performed in triplicate grown for different days to demonstrate the reproducibility. In a typical experiment, the UV sterilized cellulose–Ag nanocomposite pellets (70 mg) were placed on the agar plate, and the agar plates were incubated overnight at 37 °C. Based on the growth inhibition zones, both cotton- and MCC-Ag nanocomposites are toxic to *E. coli* and *B. subtilis*. Surprisingly, cotton supported nanocomposites are more toxic to both Gram-negative and Gram-positive species compared to the MCC supported nanocomposites (Fig. 3).

It has already been proved that the toxicity of silver nanoparticles is related to the release of Ag^+ upon oxidation of Ag NPs in the presence of water.[66] Ag^+ ions disturb several vital

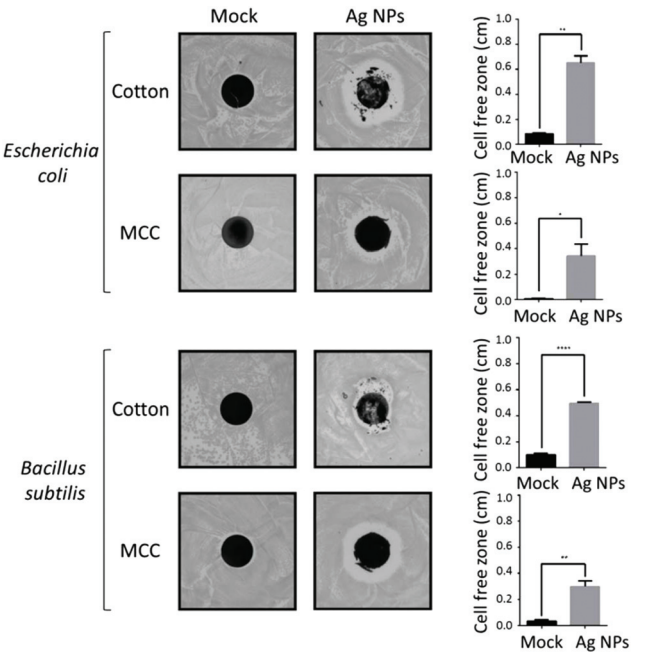

Fig. 3 Images of agar disc diffusion assays and zone of inhibition of the cotton- and MCC-Ag NPs for *E. coli* (Gram-negative) and *B. subtilis* (Gram-positive). The zone of inhibition is the mean of measurements from at least six different points. All experiments were performed in triplicate (n = 3). The graphs present the mean of 3 independent experiments. Student's *t*-test with Welch's correction was used to assess the statistical significance. (* = $p < 0.05$, ** = $P < 0.01$, *** = $P < 0.001$, **** = $P < 0.0001$). See the Experimental section for further details.

mechanisms in microorganisms.[67] The ions can block the bacterial respiration through interacting with the thiol groups in the related enzymes, and moreover, silver damages cellular metabolism, protein production, and DNA replication processes indirectly *via* producing reactive oxygen species in the cytoplasm.[68,69] In order to confirm that the Ag^+ release takes place in cotton and MCC based Ag NPs, we stored the nanocomposites in H_2O for 24 hours and performed ICP-MS measurements on the supernatant solution. Indeed, Ag^+ was present in the supernatant (Table S4†), and in the cotton-supported composites, 3.7 times more Ag^+ was released in comparison with the MCC based nanocomposites. (The concentration of Ag^+ was equal to 669.20 μg L^{-1} for the cotton-Ag NP composite and 180.82 μg L^{-1} for the MCC-Ag NP composite.)

Blends

Mechanochemical preparation can as well be used to tune the physical properties of the cellulose metal nanocomposites. Of the many physical properties, we chose to tune the contact angle (CA) of composites, since these composites may find applications in paper diagnostics where the hydrophobicity of the paper material is an important factor.[24,70] To display this tuning, cellulose–PMMA-Au and cellulose–PS-Au nanocomposites were prepared by cryomilling of the corresponding polymers with cellulose (cellulose/thermoplastic ratio equal to 1 : 1 w/w (cellulose–PS-Au **1** and cellulose–PMMA-Au **1**) and 3 : 1 w/w (cellulose–PS-Au **2** and cellulose–PMMA-Au **2**)). On the cryomilled samples, a solution of $HAuCl_4$ in H_2O (3 mL, 5.1×10^{-3} M) was introduced. Within the waiting time of 7 days, the powders changed their colour from white to purple. SEM images and EDX analysis indicated that the concentration of Au NPs was higher in the composites having a higher cellulose to polymer ratio (Fig. 4a and S25†). The formation of gold nanoparticles was additionally confirmed by XPS (Fig. S26†) and XRD (Fig. S27†) analyses. In order to check the distribution of thermoplastics in cellulose matrix elemental mapping, EDX-SEM analysis was performed (Fig. S28 and S29†). All maps confirmed the presence of C, O, and Au, which indicated that cellulose and PS or PMMA blended well with each other. A fine and equal distribution of the nanoparticles in the sample is of great importance due to further applications of the nanocomposites, which was achieved with our composites. In contrast to cellulose, polystyrene and poly (methyl methacrylate) are hydrophobic compounds; thus, their introduction into the cellulose matrix should increase the water contact angle. This was more pronounced in the case of cellulose–PS-Au nanocomposites (Fig. 4b and c). For the nanocomposite consisting of 25% of polystyrene, the contact angle was equal to 71.5° ± 4.4° (Fig. 4c). The CA increased to 86.2° ± 3.3° when the concentration of polystyrene increased to 50% (Fig. 4b). Thus, cryomilling of different ratios of cellulose and hydrophobic polystyrene enables us to achieve a continuum of desired hydrophobicities that lie in between the two extremes.[71] This tunability of hydrophobicity is essential, *e.g.*, in materials for paper diagnostics. Together with the preparation of the 'naked' metal NP in the polymer blend – free of contamination of any reducing and capping agents – through a straightforward, two-step process, this method is a promising way to obtain such 3-component-composite materials.

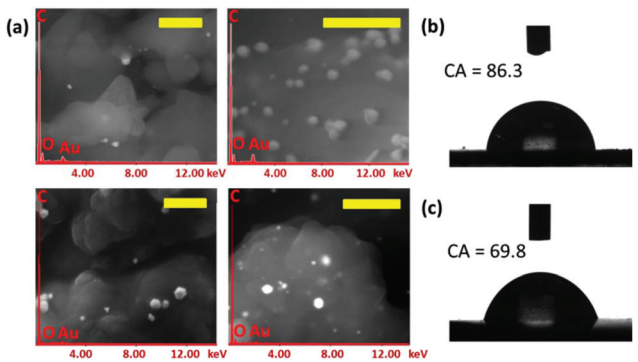

Fig. 4 (a) The EDX spectra (shown in red) of the blend nanocomposites. Cellulose–PMMA-Au and cellulose–PS-Au nanocomposites were imaged by SEM (cellulose–PMMA-Au 1, top left; cellulose–PMMA-Au 2, top right; cellulose–PS-Au 1, bottom left; and cellulose–PS-Au 2, bottom right). Scale bar = 500 nm. (b and c) Water contact angles for cellulose–PS-Au **1** and cellulose–PS-Au **2**.

Experimental

Materials

Cotton was obtained from a local pharmacy. Microcrystalline cellulose (MCC), copper(II) acetylacetonate, and 4-nitrophenol from Acros Organics were used. Chloroauric acid, palladium(II) acetylacetonate, potassium(II) tetrachloroplatinate, cobalt(II) acetylacetonate, and silver nitrate were purchased from ABCR. Sodium borohydride, polystyrene (average M_W = 280 000) and acetonitrile were purchased from Sigma-Aldrich. Poly(methyl methacrylate) (average M_W = 550 000) was purchased from Alfa Aesar. Gold, silver, platinum and palladium plasma emission standard were purchased from VWR. For the antimicrobial activity experiments, *E. coli* K-12 MG1655 strain and *B. subtilis* 168 strain were used. Sodium chloride, tryptone, yeast extract and agar powder for growth media preparation were purchased from Sigma-Aldrich.

Instrumentation

Cryomill. In all experiments, cryogenic grinding of cellulose samples was performed using a Retsch Cryomill, while cooling with liquid nitrogen from the integrated cooling system.

Scanning electron microscopy (SEM) and energy dispersive X-ray (EDX) analyses. The surface morphologies of the cellulose samples and cellulose–metal NP composites were imaged and analysed using a Quanta 200F model SEM with an accelerating voltage of 15 kV.

X-Ray photoelectron spectroscopy (XPS). XPS spectra were recorded using an ESCALAB 250 (Thermo Scientific K-Alpha X-ray photoelectron spectrometer). Photoemission was stimulated by monochromatic Al K alpha radiation (1486.6 eV).

Survey scans and high-resolution scans were performed with pass energies of 200 eV and 30 eV, respectively. Binding energies in the spectra were referenced to the C 1s binding energy set at 284.8 eV. At least three different measurements were performed for each sample.

X-Ray diffraction (XRD). XRD spectra were recorded using an X'Pert PRO, PANalytical model X-ray diffractometer with Cu Kα radiation. 40 mA current and 45 kV accelerating voltage were used.

UV-Vis spectroscopy. The absorption spectra were recorded using a Cary 100 Bio UV-Visible spectrophotometer from Varian.

ICP-MS. *For metal content calculations*: ICP-MS was recorded using a PerkinElmer Nexion 350D equipped with a cyclonic spray chamber and a glass Meinhard concentric nebulizer. The system operated with a nebulizer gas flow of 0.92 L min^{-1}, a plasma gas flow rate of 18 L min^{-1}, an auxiliary gas flow rate of 1.2 L min^{-1} and an ignition power of 1300 W.

For tracing the release of Ag^{+} from the MCC- and cotton-Ag nanocomposites: ICP-MS was recorded using a ThermoFischer Scientific XSeries 2 ICP-MS equipped with a Peltier-cooled spray chamber, a high-performance glass concentric nebulizer and a standard quartz torch. The system was operated in a peak jumping mode, at a dwell time of 10 000 ms, with a nebulizer gas flow of 0.8 L min^{-1}, sweeps per reading of 100 and an ignition power of 880 W.

Synthesis of cellulose metal nanocomposites

500 mg of cotton or MCC was cryomilled for 30 minutes at 30 Hz frequency in the presence of 6 zirconia balls (with 10.06 mm diameter) in the zirconia sample chamber at 77 K. After grinding 3 mL, 5.1×10^{-3} M of metal solution was added to the chamber and the mixture was mixed at 5 Hz for 30 seconds. Following metal solutions were used: $HAuCl_4$, K_2PtCl_4, $AgNO_3$ (in H_2O) $Co(C_5H_7O_2)_2$, $Cu(C_5H_7O_2)_2$, and $Pd(C_5H_7O_2)_2$ (in acetonitrile). Then, the mixture was diluted to 6 mL with the solvent that was used to prepare the corresponding metal solutions, placed in a polypropylene tube (VWR), and stored in the dark for 1 day, 1 week, or 2 weeks. Then, the solid was washed with solvent (H_2O or acetonitrile) and dried.

Reduction of 4-nitrophenol

Conducted in a UV cuvette: To a solution of 4-NPh in H_2O (0.30 mM, 3 mL), a solution of $NaBH_4$ in H_2O (0.47 M, 0.375 mL) was added. Then, 1.0 mg of MCC-metal NPs (total metal content: 3.76 μg (Au), 0.20 μg (Ag), 0.12 μg (Pd), and 3.22 μg (Pt), see Table S2†) was added as a catalyst. The reaction was performed in a quartz UV cuvette at room temperature and monitored using a UV-Vis spectrophotometer. Final concentrations of $NaBH_4$ and 4-NPh were 0.052 M and 0.27 mM, respectively. Standard deviation was calculated using the data from at least four independent measurements.

Conducted in the flask under constant stirring: To a solution of 4-NPh in H_2O (0.30 mM, 30 mL), a solution of $NaBH_4$ in H_2O (0.47 M, 3.75 mL) was added. Then, 10.0 mg of MCC-Au NPs was added as a catalyst. The reaction mixture was stirred in a 100 mL flask at room temperature, and after an indicated time, a small sample was taken and UV-Vis absorption spectroscopy was performed using a spectrophotometer.

Agar disk assay for the antimicrobial effect

The antimicrobial effects of cellulose–Ag nanocomposite materials on the Gram-negative (*E. coli*) and Gram-positive (*B. subtilis*) bacteria were determined using an agar disk assay. Both *E. coli* and *B. subtilis* were inoculated in a lysogeny broth (LB) and grown overnight at 37 °C. Next day, the overnight cultures were inoculated with 1 : 100 dilution in fresh media. The bacterial cultures were grown until the mid-exponential phase (OD_{600} = 0.5–0.6). For each bacteria, 5×10^6 CFU were spread onto an LB agar plate (OD_{600} = 1 taken as 10^9 CFU mL^{-1} for *E. coli* and 5×10^8 CFU mL^{-1} for *B. subtilis*). The UV sterilized cellulose Ag nanocomposite pellets (70 mg) were placed on the agar plate, and the agar plates were incubated overnight at 37 °C. The imaging was performed using a Bio-Rad Chemidoc™ imaging platform.

ICP-MS measurements

For metal content calculations: MCC-supported Au, -Pt, -Pd, and -Au (after the 1st and 2nd catalytic cycles) nanocomposites (40 mg) were dissolved in 4 mL of aqua regia, diluted to 8 mL with H_2O, centrifuged, and the supernatants were filtered. The MCC-Ag nanocomposite (40 mg) was dissolved in 3 mL of concentrated HNO_3, diluted to 6 mL with H_2O, centrifuged, and the supernatants were filtered. ICP-MS of the supernatants was performed. The reported values were the average result of 3 independent measurements.

For tracing the release of Ag^{+} from the MCC- and cotton-Ag nanocomposites: External calibration was performed by the analysis of a blank solution and five solutions of diluted Ag standard in H_2O ranging from 0 to 1000 μg L^{-1}. The cotton supported Ag nanocomposite (70 mg) and MCC supported Ag nanocomposite (70 mg) were left in 10 mL of H_2O for 24 h. After that the mixtures were centrifuged, supernatants were filtered and ICP-MS was performed. The reported values were the average result of 6 independent measurements.

Surface resistivity measurements

Surface resistivities of the cotton and metal–cotton nanocomposite pellets were measured using a two-probe method, with w = 13 mm wide samples, and the distance between the electrodes d = 100 μm. The pellets prepared for the measurements consisted of 70 mg of the nanocomposite. *I–V* plots were obtained using a Keithley electrometer (6517B), which served as the voltage source and also measured the generated current. Applied voltage was changed from 0 to 100 V in steps of 10 V and also from 0 to −100 V in steps of 10 V, which gave identical results in terms of conductivity. From the slopes of the *I–V* plots, the values were calculated for surface resistivity, R_s, according to the equation $R_s = (V/I)\cdot(w/d)$ and surface conductivity, ρ_s, $\rho_s = 1/R_s$. Standard deviations were calculated based on 5 independent measurements.

Preparation of the cellulose polymer Au blends and their metal nanocomposites

300 mg of cotton and polymer mixture (polystyrene or poly (methyl methacrylate)) was cryomilled for 30 minutes at 30 Hz frequency in the presence of 6 zirconia balls (with 10.06 mm diameter) in the zirconia sample chamber at 77 K. After grinding, 3 mL of 5.1×10^{-3} M $HAuCl_4$ solution in H_2O was added to the chamber and the mixture was mixed at 5 Hz for 30 seconds. Then, the mixture was diluted to 6 mL with H_2O, placed in a polypropylene tube, and stored in the dark for 7 days. After that, the solid was washed with H_2O and dried.

Contact angle (CA) measurements

The CAs of 3 μL water droplets on the pellet surfaces (each pellet contains 70 mg of nanocomposite) were measured 10 times for each pellet at 23 °C using the contact angle system OCA from Dataphysics.

Conclusions

In this work, cellulose–metal nanoparticle composites were prepared *via* the reduction of metal ions by cellulose mechanoradicals generated by ball milling. Gold nanoparticles were formed after 1 day of storage; however in the case of Ag, Pt, Pd, Cu, and Co, longer storage times were necessary to achieve higher concentrations of NPs. A great advantage of this method is the elimination of hazardous reducing and stabilizing agents used in the conventional synthesis. The presence of metal NPs in the cellulose matrix also increased the electrical surface conductivity of the nanocomposites in comparison with the native cellulose. Moreover, MCC-Au, -Ag, -Pt, and -Pd NPs were involved in the catalytic transformation of 4-nitrophenolate into 4-aminophenolate. Reactions occurred fast with satisfactory rate constants. Thus, cellulose acts as a good supporting matrix for nanoparticles and provides good access to 'naked' metal NPs. In addition, the antimicrobial activity of cellulose–Ag nanocomposites determined using an agar disk assay against *E. coli* and *B. subtilis* showed that both cotton- and MCC-Ag nanocomposites were toxic to the Gram-positive and Gram-negative bacteria. Finally, cellulose–PS-Au and cellulose–PMMA-Au nanocomposites were prepared with a varying ratio of cellulose to thermoplastic polymer. On introducing polystyrene into the cellulose matrix, the hydrophobicity of the nanocomposite increased.

To conclude, with this study we have shown a straightforward and green access to 'naked' (without any stabilizer) nanoparticle synthesis with milling of cellulose, which takes place without any reducing agent other than the cellulose mechanoradicals produced in the milling process. We hope that this study serves as an example for the green production of cellulose nanocomposites, which are gaining an accelerated interest in newly emerging fields such as paper diagnostics and paper electronics.

Author contributions

B. B. conceived the project idea, supervised and coordinated the work. J. K.-Y., M. D. and Ö. L. carried out the experiments. R. E. A. carried out the antimicrobial tests under the supervision of U. Ş. J. K.-Y. and B. B. wrote the manuscript. All authors have given approval to the final version of the manuscript.

Conflicts of interest

There are no conflicts to declare.

Acknowledgements

This work was supported by the Scientific and Technological Research Council of Turkey (TÜBİTAK) under the project number 115Z452. We thank Cangül Aktürk for the ICP-MS measurements.

References

1 A. C. O'sullivan, *Cellulose*, 1997, **4**, 173–207.
2 R. J. Moon, A. Martini, J. Nairn, J. Simonsen and J. Youngblood, *Chem. Soc. Rev.*, 2011, **40**, 3941–3994.
3 S. Kalia, A. Dufresne, B. M. Cherian, B. S. Kaith, L. Avérous, J. Njuguna and E. Nassiopoulos, *Int. J. Polym. Sci.*, 2011, **2011**, 1–35.
4 M. A. S. Azizi Samir, F. Alloin and A. Dufresne, *Biomacromolecules*, 2005, **6**, 612–626.
5 S. Ummartyotin and H. Manuspiya, *Renewable Sustainable Energy Rev.*, 2015, **41**, 402–412.
6 Q. Yuan, D. Wu, J. Gotama and S. Bateman, *J. Thermoplast. Compos. Mater.*, 2008, 195–208.
7 D. K. Bhat and M. S. Kumar, *J. Polym. Environ.*, 2006, **14**, 385–392.
8 R. Mahmood Raouf, Z. Abdul Wahab, N. Azowa Ibrahim, Z. Abidin Talib and B. W. Chieng, *Polymer*, 2016, **8**, 128.
9 C.-N. Wu, T. Saito, Q. Yang, H. Fukuzumi and A. Isogai, *ACS Appl. Mater. Interfaces*, 2014, **6**, 12707–12712.
10 Z. Pang, Z. Yang, Y. Chen, J. Zhang, Q. Wang, F. Huang and Q. Wei, *Colloids Surf., A*, 2016, **494**, 248–255.
11 A. Kafy, A. Akther, Md. I. R. Shishir, H. C. Kim, Y. Yun and J. Kim, *Sens. Actuators, A*, 2016, **247**, 221–226.
12 S. Mun, H. C. Kim, H.-U. Ko, L. Zhai, J. W. Kim and J. Kim, *Sci. Technol. Adv. Mater.*, 2017, **18**, 437–446.
13 R. Barras, I. Cunha, D. Gaspar, E. Fortunato, R. Martins and L. Pereira, *Flexible Printed Electron.*, 2017, **2**, 014006.
14 S. Majumdar and B. Adhikari, *Bull. Mater. Sci.*, 2005, **28**, 703–712.
15 J.-M. Raquez, Y. Habibi, M. Murariu and P. Dubois, *Prog. Polym. Sci.*, 2013, **38**, 1504–1542.

16 J. Hinestroza and A. N. Netravali, *Cellulose Based Composites*, Wiley-VCH Verlag GmbH & Co. KGaA, Weinheim, Germany, 2014.
17 S. K. Murthy, *Int. J. Nanomed.*, 2007, **2**, 129–141.
18 O. Salata, *J. Nanobiotechnol.*, 2004, **2**, 3.
19 C. S. C. Santos, B. Gabriel, M. Blanchy, O. Menes, D. García, M. Blanco, N. Arconada and V. Neto, *Mater. Today: Proc.*, 2015, **2**, 456–465.
20 M. J. Hajipour, K. M. Fromm, A. A. Ashkarran, D. Jimenez de Aberasturi, I. R. de Larramendi, T. Rojo, V. Serpooshan, W. J. Parak and M. Mahmoudi, *Trends Biotechnol.*, 2012, **30**, 499–511.
21 S. Prabhu and E. K. Poulose, *Int. Nano Lett.*, 2012, **2**, 32.
22 Y. Lee, J.-R. Choi, K. J. Lee, N. E. Stott and D. Kim, *Nanotechnology*, 2008, **19**, 415604.
23 Y. Yang, Q. Huang, G. F. Payne, R. Sun and X. Wang, *Nanoscale*, 2019, **11**, 725–732.
24 M. M. Gong and D. Sinton, *Chem. Rev.*, 2017, **117**, 8447–8480.
25 S. Wang, J. Sun, Y. Jia, L. Yang, N. Wang, Y. Xianyu, W. Chen, X. Li, R. Cha and X. Jiang, *Biomacromolecules*, 2016, **17**, 2472–2478.
26 M. R. de Moura, L. H. C. Mattoso and V. Zucolotto, *J. Food Eng.*, 2012, **109**, 520–524.
27 M. Kaushik and A. Moores, *Green Chem.*, 2016, **18**, 622–637.
28 E. Lam, S. Hrapovic, E. Majid, J. H. Chong and J. H. T. Luong, *Nanoscale*, 2012, **4**, 997–1002.
29 H. Koga, E. Tokunaga, M. Hidaka, Y. Umemura, T. Saito, A. Isogai and T. Kitaoka, *Chem. Commun.*, 2010, **46**, 8567–8569.
30 X. Wu, C. Lu, Z. Zhou, G. Yuan, R. Xiong and X. Zhang, *Environ. Sci.: Nano*, 2014, **1**, 71–79.
31 X. Wu, C. Lu, W. Zhang, G. Yuan, R. Xiong and X. Zhang, *J. Mater. Chem. A*, 2013, **1**, 8645–8652.
32 J. Tang, Z. Shi, R. M. Berry and K. C. Tam, *Ind. Eng. Chem. Res.*, 2015, **54**, 3299–3308.
33 D. G. Capco and Y. Chen, *Nanomaterial. Impacts on Cell Biology and Medicine*, Springer, 2014.
34 N. C. T. Martins, C. S. R. Freire, R. J. B. Pinto, S. C. M. Fernandes, C. P. Neto, A. J. D. Silvestre, J. Causio, G. Baldi, P. Sadocco and T. Trindade, *Cellulose*, 2012, **19**, 1425–1436.
35 S. Ifuku, M. Tsuji, M. Morimoto, H. Saimoto and H. Yano, *Biomacromolecules*, 2009, **10**, 2714–2717.
36 S. Boufi, A. M. Ferraria, A. M. B. do Rego, N. Battaglini, F. Herbst and M. R. Vilar, *Carbohydr. Polym.*, 2011, **86**, 1586–1594.
37 I. Díez, P. Eronen, M. Österberg, M. B. Linder, O. Ikkala and R. H. A. Ras, *Macromol. Biosci.*, 2011, **11**, 1185–1191.
38 W. K. Son, J. H. Youk and W. H. Park, *Carbohydr. Polym.*, 2006, **65**, 430–434.
39 G. Mary, S. K. Bajpai and N. Chand, *J. Appl. Polym. Sci.*, 2009, **113**, 757–766.
40 J. He, T. Kunitake and A. Nakao, *Chem. Mater.*, 2003, **15**, 4401–4406.
41 K. Pirkkalainen, K. Leppänen, U. Vainio, M. A. Webb, T. Elbra, T. Kohout, A. Nykänen, J. Ruokolainen, N. Kotelnikova and R. Serimaa, *Eur. Phys. J. D*, 2008, **49**, 333–342.
42 J. Andersen and J. Mack, *Green Chem.*, 2018, **20**, 1435–1443.
43 M. N. Temnikov, A. A. Anisimov, P. V. Zhemchugov, D. N. Kholodkov, A. S. Goloveshkin, A. V. Naumkin, S. M. Chistovalov, D. Katsoulis and A. M. Muzafarov, *Green Chem.*, 2018, **20**, 1962–1969.
44 E. Colacino, A. Porcheddu, I. Halasz, C. Charnay, F. Delogu, R. Guerra and J. Fullenwarth, *Green Chem.*, 2018, **20**, 2973–2977.
45 S. Menuel, B. Léger, A. Addad, E. Monflier and F. Hapiot, *Green Chem.*, 2016, **18**, 5500–5509.
46 M. J. Rak, N. K. Saadé, T. Friščić and A. Moores, *Green Chem.*, 2013, **16**, 86–89.
47 M. J. Rak, T. Friščić and A. Moores, *Faraday Discuss.*, 2014, **170**, 155–167.
48 M. Baláž, N. Daneu, Ľ. Balážová, E. Dutková, Ľ. Tkáčiková, J. Briančin, M. Vargová, M. Balážová, A. Zorkovská and P. Baláž, *Adv. Powder Technol.*, 2017, **28**, 3307–3312.
49 M. Sakaguchi, T. Ohura, T. Iwata and Y. Enomoto-Rogers, *Polym. Degrad. Stab.*, 2012, **97**, 257–263.
50 T. Ohura, Y. Tsutaki and M. Sakaguchi, *Sci. World J.*, 2014, **2014**, 127506.
51 F. Zhang, W. Qiu, L. Yang, T. Endo and T. Hirotsu, *J. Mater. Chem.*, 2002, **12**, 24–26.
52 X. Meng, X. Bi, C. Yu, G. Chen, B. Chen, Z. Jing and P. Zhao, *Green Chem.*, 2018, **20**, 4638–4644.
53 X. Meng, X. Bi, G. Chen, B. Chen and P. Zhao, *Org. Process Res. Dev.*, 2018, **22**, 1716–1722.
54 M. Sakaguchi, M. Makino, T. Ohura and T. Iwata, *J. Phys. Chem. A*, 2012, **116**, 9872–9877.
55 H. T. Baytekin, B. Baytekin and B. A. Grzybowski, *Angew. Chem., Int. Ed.*, 2012, **51**, 3596–3600.
56 M. Sakaguchi, T. Ohura, T. Iwata, S. Takahashi, S. Akai, T. Kan, H. Murai, M. Fujiwara, O. Watanabe and M. Narita, *Biomacromolecules*, 2010, **11**, 3059–3066.
57 H. T. Baytekin, B. Baytekin, T. M. Hermans, B. Kowalczyk and B. A. Grzybowski, *Science*, 2013, **341**, 1368–1371.
58 H. T. Baytekin, B. Baytekin, S. Huda, Z. Yavuz and B. A. Grzybowski, *J. Am. Chem. Soc.*, 2015, **137**, 1726–1729.
59 B. Baytekin, H. T. Baytekin and B. A. Grzybowski, *J. Am. Chem. Soc.*, 2012, **134**, 7223–7226.
60 Ö. Laçin, J. Kwiczak-Yiğitbaşı, M. Erkan, Ş. C. Cevher and B. Baytekin, *Polym. Degrad. Stab.*, 2019, **168**, 108945.
61 R. J. B. Pinto, M. C. Neves, C. P. Neto and T. Trindade, *Nanocomposites - New Trends and Developments*, IntechOpen, 2012.
62 R. Robert, S. Barbati, N. Ricq and M. Ambrosio, *Water Res.*, 2002, **36**, 4821–4829.
63 N. Pradhan, A. Pal and T. Pal, *Colloids Surf., A*, 2002, **196**, 247–257.
64 X. Lin, M. Wu, D. Wu, S. Kuga, T. Endo and Y. Huang, *Green Chem.*, 2011, **13**, 283–287.
65 S. Adepu and M. Khandelwal, *J. Mater. Sci.*, 2018, **53**, 1596–1609.

66 Z. Xiu, Q. Zhang, H. L. Puppala, V. L. Colvin and P. J. J. Alvarez, *Nano Lett.*, 2012, **12**, 4271–4275.
67 J. L. J. Graves, M. Tajkarimi, Q. Cunningham, A. Campbell, H. Nonga, S. H. Harrison and J. E. Barrick, *Front. Genet.*, 2015, **6**, 42.
68 K. Mijnendonckx, N. Leys, J. Mahillon, S. Silver and R. Van Houdt, *BioMetals*, 2013, **26**, 609–621.
69 Q. L. Feng, J. Wu, G. Q. Chen, F. Z. Cui, T. N. Kim and J. O. Kim, *J. Biomed. Mater. Res.*, 2000, **52**, 662–668.
70 H. T. Baytekin, T. Wirth, T. Gross, M. Sahre, W. E. S. Unger, J. Theisen and M. Schmidt, *Surf. Interface Anal.*, 2010, **42**, 1417–1431.
71 X. Li, D. R. Ballerini and W. Shen, *Biomicrofluidics*, 2012, **6**, 011301.